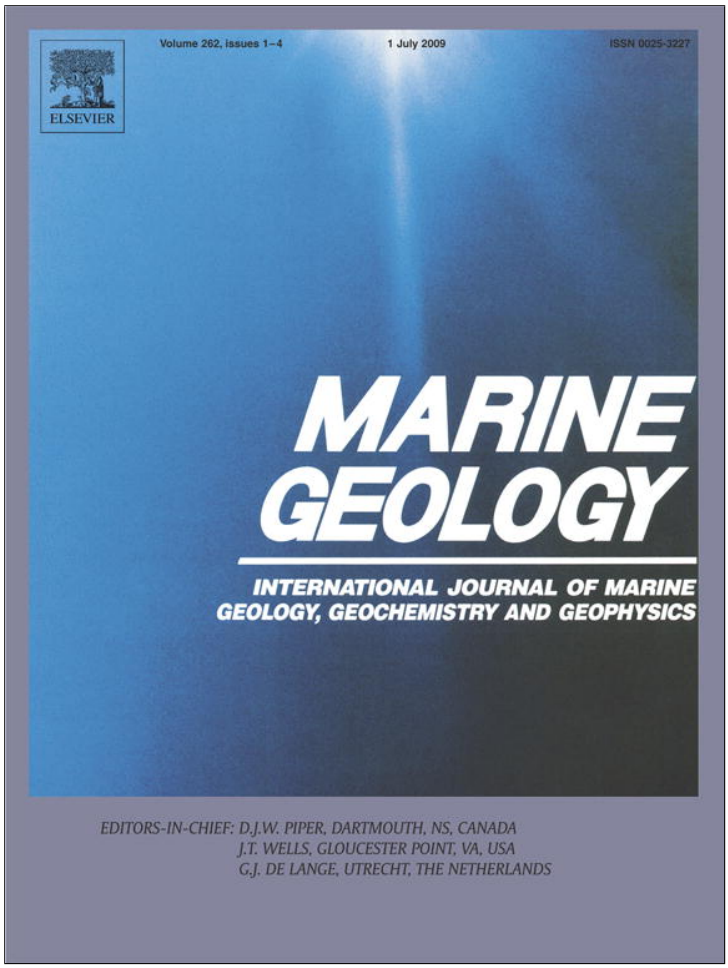

Marine Geology 262 (2009) 50–61

Contents lists available at ScienceDirect

Marine Geology

journal homepage: www.elsevier.com/locate/margeo

Geochemical and diatom signatures of bottom water renewal events in Effingham Inlet, British Columbia (Canada)

Murray B. Hay [a,*], Stephen E. Calvert [b], Reinhard Pienitz [a], Audrey Dallimore [c], Richard E. Thomson [d], Timothy R. Baumgartner [e]

[a] Aquatic Paleoecology Laboratory, Département de géographie et Centre d'études nordiques, Université Laval, Québec, Québec, Canada G1V 0A6
[b] Department of Earth and Ocean Sciences, University of British Columbia, 6270 University Boulevard, Vancouver, British Columbia, Canada V6T 1Z4
[c] Geological Survey of Canada, GSC Pacific - Sidney Subdivision, P.O. Box 6000 Sidney, BC, Canada V8L 4B2
[d] Institute of Ocean Sciences, Sidney, British Columbia, Canada V8L 4B2
[e] División de Oceanología, Centro de Investigacíon Científica y Educacíon Superior de Ensenada, Ensenada, Baja California, Mexico

ARTICLE INFO

Article history:
Received 23 May 2008
Received in revised form 8 January 2009
Accepted 8 March 2009
Available online xxxx

Communicated by G.J. de Lange

Keywords:
diatoms
fjords
geochemistry
carbon isotopes
sedimentation
paleoceanography

ABSTRACT

Sediments from Effingham Inlet, Vancouver Island, British Columbia hold a valuable high-resolution Holocene record of paleoclimatic and paleoceanographic conditions in the northeast Pacific Ocean. Accurate interpretation of this record requires that the depositional environment be well understood. In order to assess deposition within the fjord over the last 1500 years, two cores, a Soutar box core and a Kasten core, were analyzed for fossil diatoms, and biogeochemical properties. The cores contain varved sequences intercalated with homogeneous mud layers and a seismite. We show that homogeneous mud units related to periods of bottom water renewal are geochemically distinct from the seismite and that these bottom renewal events are favored when brackish rather than marine surface water conditions are present. The seismite, deposited in AD 1946, has lower opal and higher organic carbon concentrations and higher organic carbon: nitrogen ratios reflecting greater terrestrial material input. In contrast, homogeneous mud units are marked by a lower organic C/N and more isotopically heavy $\delta^{13}C$ values, suggesting a stronger marine influence. Major metals and trace element data also confirm that the source material of these units differs from that of the AD 1946 seismite. Fossil diatom assemblages within the homogeneous mud units are characterized by a decreased abundance of typical marine spring bloom taxa (*Skeletonema costatum*, *Chaetoceros* spp., *Thalassiosira* spp.) coupled with an increased abundance of the brackish-water taxon *Cyclotella choctawhatcheeana*. Reduced surface salinity enhances stratification of the water column which, in turn, favors an intensified two-layer estuarine exchange across the shallow sills and associated bottom water renewal. The homogeneous mud units are produced through transport of sediment into the fjord coupled with a reworking of the upper layers of the sediment column. Therefore, these units represent a recorder of past changes in regional oceanography and climate.

1. Introduction

As coastal environments experiencing high sedimentation rates, fjords represent potentially useful sites for the reconstruction of both past terrestrial and oceanic conditions (Syvitski and Shaw, 1995). Adjacent to the open ocean, these inlets are natural sediment traps serving as recorders of past environmental conditions along ocean margins (e.g. McMinn et al., 2001; Jensen et al., 2004). Furthermore, the bathymetry of fjords, coupled with an elevated primary production, often favors the formation of anoxic bottom waters and the preservation of annually-laminated (varved) sequences (e.g. Chang et al., 2003).

Effingham Inlet, a small fjord along the west coast of Vancouver Island, British Columbia (B.C.), is an excellent site for high-resolution paleoceanographic research (Chang et al., 2003; Dallimore et al., 2005; Hay et al., 2007; Ivanochko et al., 2008). With an anoxic inner basin and an adjacent suboxic-anoxic outer basin, sediment records from the inlet are mainly composed of diatom-mud varves (Chang et al., 2003; Dallimore et al., 2005). Furthermore, the inlet faces the open ocean and an area of important upwelling (McFarlane et al., 1997). This favors preservation of a distinct offshore oceanographic signal within the sediment record of the inlet (Hay et al., 2007).

As with other fjords, Effingham Inlet is a steep-sided basin with a relatively complex depositional setting. As a result, it is subject to a number of sedimentary processes that require proper identification for accurate interpretation of past environmental conditions. This is especially critical in tectonically active regions, such as the west

* Corresponding author. Present address: Département des Sciences Humaines, Université du Québec à Chicoutimi, 555 boulevard de l'Université, Chicoutimi, Québec, Canada G7H 2B1. Tel.: +1 418 545 5011x5673; fax: +1 418 615 1207.
E-mail addresses: Murray_Hay@uqac.ca (M.B. Hay), calvert@eos.ubc.ca (S.E. Calvert), Reinhard.Pienitz@cen.ulaval.ca (R. Pienitz), adallimore@NRCan.gc.ca (A. Dallimore), Richard.Thomson@dfo-mpo.gc.ca (R.E. Thomson), tbaumgar@cicese.mx (T.R. Baumgartner).

0025-3227/$ – see front matter © 2009 Elsevier B.V. All rights reserved.
doi:10.1016/j.margeo.2009.03.004

coast of British Columbia (Blais-Stevens and Clague, 2001; Dallimore et al., 2005; Dallimore et al., 2009).

Sediments recovered from the inlet consist of annually laminated diatomaceous silty clays (varves) with occasional intercalations of various types of unstructured or homogeneous silty clays (Chang et al., 2003; Dallimore et al., 2005). The non-laminated units range in thickness from a few millimetres to more than 50 cm. Early studies of laminated sediments in B.C. fjords interpreted most non-laminated units in the sediment column as seismites, namely proxies for disturbance related to seismic events or as the result of debris flows generated by over-steepening of sediment that had accumulated along the fjord walls (Blais-Stevens et al., 1997). However, further studies have shown that some non-laminated, homogeneous mud units within the laminated sediments of anoxic B.C. fjords are not related to seismic events, yet represent indicators of paleoenvironmental conditions (Dallimore et al., 2005; Dallimore et al., 2009).

These homogeneous mud units are interpreted to have formed by re-suspension of previously laminated sediments by bottom currents flowing over the sill into the inner basin of the inlet during re-oxygenation events. Bottom water renewal in coastal inlets along the British Columbia coast is often accompanied by an increased sediment flux to the deeper portion of the basins (Timothy et al., 2003). This renewal in Effingham Inlet requires a "preconditioning" of the waters inside and outside the anoxic basins, including enhanced stratification of the upper water column, intensified estuarine circulation, a decrease in deep water density due to vertical diffusive processes, and/or increased coastal upwelling (Dallimore et al., 2005). Bottom water renewal events in the inlet appear to last a maximum of a few months before anoxic conditions return (Patterson et al., 2000).

In this paper, we utilize geochemical and microfossil tools for distinguishing between seismites and homogeneous mud units related to bottom-water renewal. We analyze two continuously sampled sediment cores, representing 1500 years of sedimentation, recovered from the inner basin of Effingham Inlet. In this paper we compare the geochemical signature of a known earthquake-related sediment deposit (seismite) with that of the homogeneous mud units in order to identify the sources of the biogenous and lithogenous material within the sedimentary units of Effingham Inlet. We then examine the fossil diatom assemblages (class: Bacillariophyceae) to highlight the oceanic and climatic conditions responsible for bottom water renewal and the formation of homogeneous mud units in the inlet.

2. Study site

Effingham Inlet is a 17-km long fjord located in the northeastern corner of Barkley Sound on the west coast of Vancouver Island (Fig. 1). The narrow inlet, with an average width of 1 km, is characterized by the presence of two suboxic to anoxic basins. An inner sill with a depth of 40 m separates the inner and outer basins, with depths of 125 m and 205 m, respectively (Patterson et al., 2000). The outer basin is separated from Barkley Sound by a sill having a minimum depth of 60 m. Barkley Sound opens directly to the Pacific Ocean and has an irregular bathymetry with an average depth of 70 m. The sides of the fjord are steep and are covered by a coastal temperate rainforest. Littoral marsh areas are restricted to narrow zones at the base of the fjord walls and to a few areas concentrated around the fjord head and outer basin (Fig. 1B).

Pickard (1963) classified Effingham Inlet as a low runoff fjord. The predominant freshwater source, the Effingham River, enters at the head of the fjord with an estimated mean flow of 6 to 8 m^3s^{-1} and maximum mean monthly discharge of 14 m^3s^{-1} (Stronach et al., 1993). Peak freshwater discharge into Effingham Inlet occurs during late fall and early winter (October–January) when annual precipitation is at a maximum. Winter temperatures usually remain above freezing at lower elevations, preventing a large amount of snow accumulation, thereby limiting the spring freshet typical of most mainland fjord systems.

The limited freshwater input produces a weak estuarine circulation during the summer months. Weak estuarine circulation coupled with weak tidal currents favor the development of suboxic–anoxic conditions at the bottom of the fjord (Patterson et al., 2000). Freshwater input from the Effingham River forms a thin lens of brackish surface water in the inner fjord. The salinity of this layer increases rapidly seaward through vertical mixing with the salty water beneath. This outflow, and accompanying loss of salt as a result of vertical entrainment from underlying waters, is compensated by inflow within a relatively warm (>10 °C) intermediate-depth layer with salinities ranging from 29.0 to 32.0. This layer, likely representing upwelled offshore waters that have mixed with the bottom waters of the Vancouver Island Coastal Current (Fig. 1), penetrates into Effingham Inlet in mid- to late summer and reaches the innermost portions of the inlet by late fall. Depending on temperature and salinity distributions within the basins at the time of intermediate to deep water intrusion into the inlet, denser deep water (<9 °C and salinity >32.3) entering the two basins can extend from the shallow inner and outer sills downslope to the sea floor. Oxygenated upwelled waters are able to penetrate into the fjord and, if sufficiently dense relative to the deep waters in the basins, will occasionally renew the bottom waters. Although renewal events typically affect both the inner and outer basins, some events are too weak to penetrate from the outer into the inner basin.

3. Materials and methods

A Soutar box core (EFBC9703-2) and Kasten core (EFKC9703-1) (Kogler, 1963) were recovered from the inner basin of Effingham Inlet at depths of 122 m and 120 m, respectively (Fig. 1B). Core material was recovered and transported to Scripps Institution of Oceanography (SIO), La Jolla, CA and were kept in cool (4 °C) storage for 2 years. After draining, the box and Kasten cores had lengths of 73 cm and 197 cm, respectively. The cores were cut into a number of slabs and X-rayed using SIO standard slab preparation techniques. Slabs were X-rayed with a 40 kV, 40 Ma belt-feed X-ray machine using Kodak™ XTL-2 X-ray film.

Preliminary inspection of the X-ray radiographs showed three principal units in the Soutar box core: (1) a laminated sequence underlain by (2) a massive (homogeneous) unit, and (3) a basal unit of distorted laminae. Based on the X-ray plates, the upper section of the box core was sampled every two laminar couplets. The sediment gravity flow unit located immediately below the laminae was sampled at 1-cm intervals. Disturbed laminae below the massive unit were sampled at approximately 2-cm intervals, following the laminar planes.

Sampling of the Kasten core was based on laminae patterns and homogeneous mud units identified in the X-ray images. Laminae and disturbed laminae sequences were sampled at <1-cm intervals. Homogeneous mud sections within the core were sampled at 1-cm intervals.

3.1. Radiometric analyses

All ^{137}Cs and ^{210}Pb analyses of cores EFBC9703-2 and EFKC9703-1 were conducted at GEOTOP, Université de Québec à Montréal. Values for ^{137}Cs and ^{210}Pb were corrected for salt content. Lead-210 estimates were made from the activity of the radioactive daughter product ^{210}Po using alpha spectrometry and ^{210}Pb values were back calculated to the time of coring. The chronology was estimated using a constant rate of supply (CRS) ^{210}Pb model (Binford, 1990).

For all radiocarbon dating, AMS techniques used predominantly wood samples and a single marine shell. Samples were analyzed at BETA Laboratories, Florida (BETA-2 samples) and the Keck Carbon Cycle AMS Facility, Earth System Science Department, University of California at Irvine (UCIAMS-12 samples). All dates were calibrated to calendar years using INTCAL98 (Stuiver et al., 1998a) for wood samples and MARINE98 (Stuiver et al., 1998b) for shell material. A regional marine reservoir

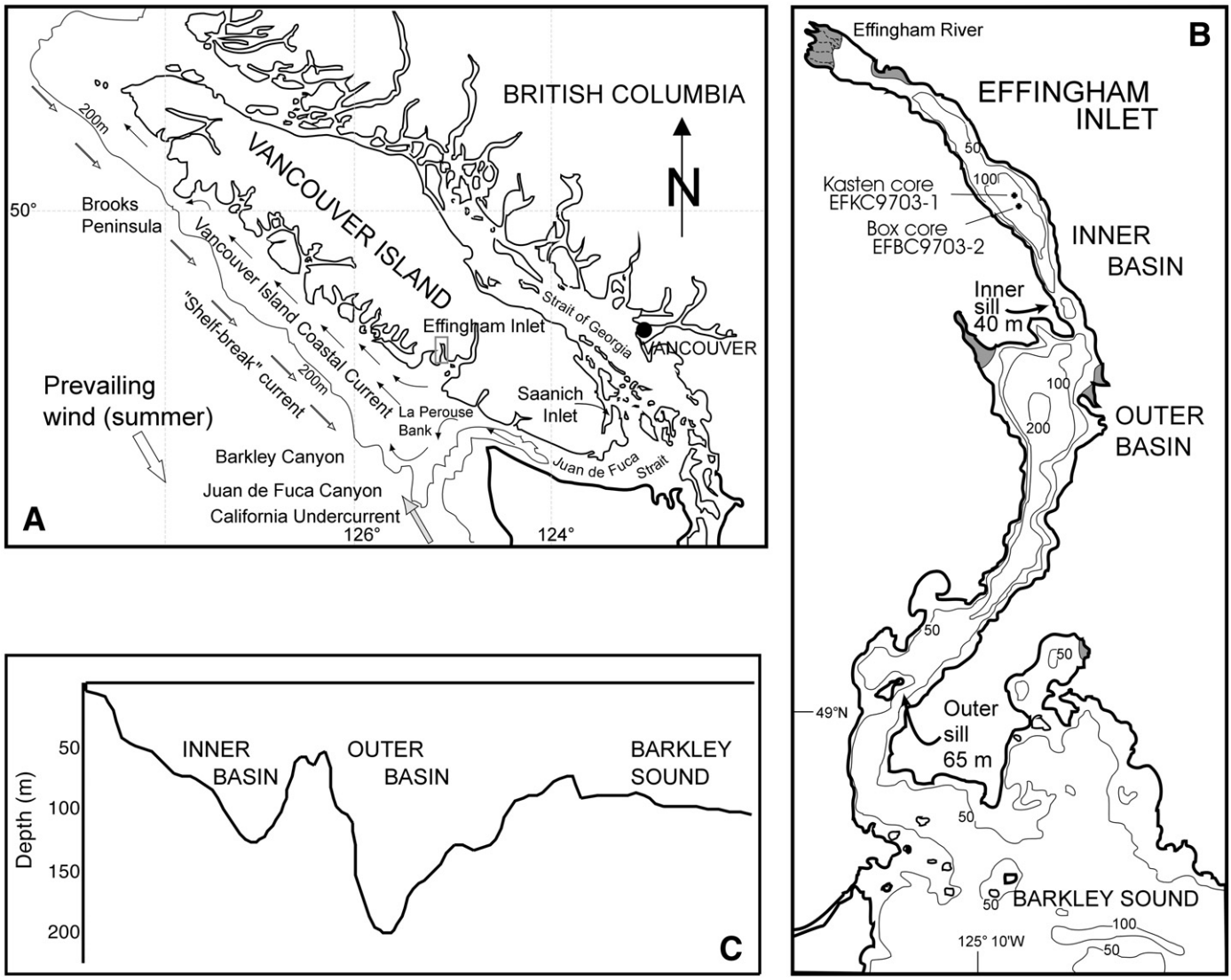

Fig. 1. Location of Effingham Inlet, British Columbia, Canada. A) Southern coastal British Columbia with locations referred to in the text as well as the positions of oceanic currents along the west coast of Vancouver Island during the summer months (modified from Thomson et al., 1989). Strong upwelling occurs in the La Perouse Bank region southwest of Barkley Sound. Rectangle indicates study area shown in B. B) Effingham Inlet with locations of sampling stations. Bathymetric contours in metres. C) Cross-section of Effingham Inlet with vertical exaggeration (modified from Hay et al., 2003).

correction of $\Delta R = 390 \pm 25$ years was applied to the shell material using the program CALIB (Stuiver and Reimer, 1993) version 5.0.2.

3.2. Diatom preparation

Diatom preparation and absolute abundance estimates followed those detailed in Hay et al. (2003). In brief, approximately 20 mg of freeze-dried sediment were added to a scintillation vial. A few drops of 10% HCl and a maximum of 4 mL of 35% hydrogen peroxide (H_2O_2) were added to each vial. The vials were placed on a hot plate and the reaction was allowed to continue until the slurry was transparent. The vials were decanted and then refilled with distilled water at 24-hour intervals for 5 days.

Coverslips measuring 18 × 18 mm square were pipetted with 500 μL of slurry and were left to dry at room temperature. Coverslips were mounted using the high refractive mounting medium Naphrax® (refractive index = 1.78). Sediment and slurries are archived at the Canadian Museum of Nature, accession number: CANA 72741-73451.

Diatoms were identified to the lowest taxonomic level possible (e.g. variety) at a magnification of 1000x using a Leica DMRB microscope. Counting rules followed those outlined in Schrader and Gersonde (1978). Vegetative frustules of *Chaetoceros* were rare, usually found with the setae detached from the valve, and were included with *Chaetoceros* resting spore (r. sp.) counts. A minimum of 500 valves were counted not including *Chaetoceros* r. sp. or silicoflagellates.

3.3. Geochemical analyses

Prior to geochemical analyses, all sediment samples were freeze-dried and then manually ground into fine powders in an agate mortar. Total carbon and nitrogen were determined by combustion-gas chromatography (Fisons 1500 CHN elemental analyzer) with precisions of ± 1.2% and ± 3.0%, respectively, and carbonate carbon was determined by coulometry following acid evolution of CO_2 with a precision of ± 3.7%. Organic carbon was estimated by difference (total carbon minus carbonate carbon) with a combined precision of ± 3.9%. Biogenous silica (opal) was determined by molybdenum blue spectrophotometry following Na_2CO_3 dissolution (Mortlock and Froelich, 1989) with a precision of ± 5%.

Major and minor element concentrations were determined by X-ray fluorescence spectrometry using methods described by Calvert et al. (2001). Precision was ± 3% for major elements and ± 5% for

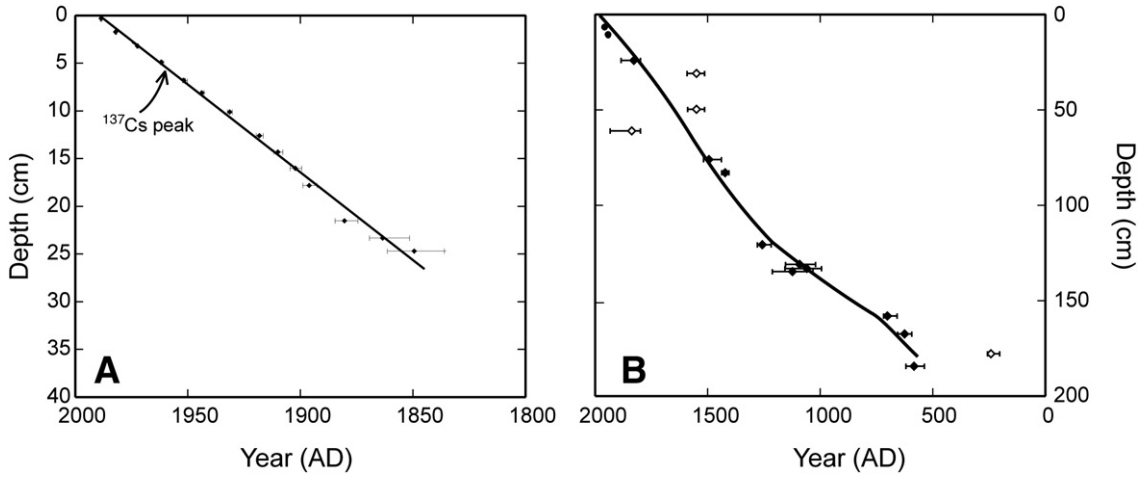

Fig. 2. Age-depth curves for the box core EFBC9703-2 and Kasten core EFKC9703-1. A) Dating of the box core based on excess ^{210}Pb and a constant rate of supply model (CRS) (Binford, 1990) as well as ^{137}Cs. The seismite, representing the instantaneous deposition of material, was excised from the age-depth model. B) Dating of the Kasten core was based on ^{14}C dating as well as two diatom biomarker horizons (*Rhizosolenia* – ca. AD 1940 and *Minidiscus chilensis* – AD 1860: filled circles). Radiocarbon dates used for the age-depth model are marked by filled triangles and those not included in the age-depth model are represented by transparent triangles.

minor elements. International reference samples (USGS, Japan Geological Survey, Canada Center for Mineral and Energy Technology, National Institute for Metallurgy, South Africa) were used for calibration, and a separate sub-set of these standards were run as accuracy monitors throughout the determinations. Precisions were better than ±1.5% for the major elements and better than ±3% for all minor elements except Zr (±4%) and Cu (±5%). Estimates of lithogenous calcium (%Ca) were calculated by difference on a carbonate-free basis (%Ca_{total} minus %$Ca_{carbonate}$), and lithogenous silicon (%Si) was estimated as %Si_{total} minus %Si_{opal}.

The salt content of the samples were determined by titrimetric chlorinity analysis of distilled water leachates of 50 mg subsamples. The results were used to correct for the diluting effect of sea water salts in the dried bulk samples and for the contributions of Ca, Mg, K, Na and Sr to the elemental values from occluded salt. Organic carbon, carbonate, total nitrogen and opal concentrations were also corrected for salt content.

Organic carbon isotope ratios in bulk sediment were determined using a Carlo Erba CHN analyser connected on-line to a VG PRISM isotope ratio mass spectrometer. Sediments were de-carbonated using 10% HCl and dried, without removing excess acid, prior to analysis. Results are reported as δ^{13}C relative to the VPDB standard and the precision was ±0.2‰.

4. Results

4.1. Chronological framework

Cesium-137 and ^{210}Pb dating provided ages of ca. AD 1990 and ca. AD 1855 for the top and bottom of the box core EFBC9703-2, respectively (Fig. 2A). Details of ^{210}Pb dating of the box core are presented in Hay (2005). A total of 38 varves were counted above the massive unit with the uppermost portion of the core marked by indistinct laminae (Hay, 2005). As the uppermost portion of the box core was lost upon recovery (Diego Holmgren, University of Washington, Seattle, written communication, 2001), a core top date of ca. AD 1990 was estimated from sedimentation rates of the preserved varves and comparison of ^{210}Pb concentrations in the box core and a freeze core (TUL99B04) also recovered from the inner basin (Chang, 2004). The 1963 ^{137}Cs peak was observed at 6.0 cm depth, 16–17 varves above the 40-cm thick massive unit. In addition, the absence of ^{137}Cs within the four varves situated immediately above the massive unit show that these sediments are younger than AD 1952. Similar results were obtained by analysis of the freeze core TUL99B04 (Chang, 2004). Varve counts and the position of the ^{137}Cs peak therefore show that deposition of the massive unit occurred ca. AD 1946.

Dating control of the Kasten core EFKC9703-1 relied on 14 radiocarbon dates (Table 1; Fig. 2B), ^{210}Pb activity and utilization of diatom

Table 1
Radiocarbon dates along Kasten core EFKC9703-1, inner basin of Effingham Inlet.

Laboratory code	Material dated	Core depth (cm)	^{14}C age with error	δ^{13}C	Calibrated age range year AD	Relative probability under curve	Median probable calibrated year AD
UCIAMS-4700	Leaf - *Thuja*?	33.2	130±20	−26.8	1800–1891	0.491	1833
UCIAMS-4699	Wood fragments	40.2	300±20	28.5	1515–1598	0.723	1556
UCIAMS-4698	Wood fragments	59	295±20	−21.1	1517–1594	0.691	1556
Beta-160727	Twig	70.4	70±50	−25.1	1801–1938	0.684	1840
UCIAMS-4697	Leaf - *Thuja*?	85.5	380±25	−23.5	1446–1523	0.7	1494
UCIAMS-4695	Wood fragments	92.2	490±20	−26.4	1413–1443	1	1428
UCIAMS-4694	Leaf	130.1	770±20	−28.8	1223–1276	1	1256
UCIAMS-4693	Bark	140.5	940±25	−26	1029–1156	1	1097
Beta-156838	Shell valve - *Mytilus edulis*	142.6	1730±30	−0.9	983–1174	1	1067
UCIAMS-4692	Seed	144.3	895±35	−30.6	1039–1215	1	1130
UCIAMS-4690	Pine cone	167.5	1305±20	−26.4	661–721	0.7	695
UCIAMS-4689	Twig	177.1	1430±20	−28.6	594–654	1	625
UCIAMS-4688	Pine needles	187.3	1785±25	−25.6	136–262	0.724	240
UCIAMS-4687	Pine cone	193.9	1480±20	−22.7	548–632	1	586

Radiocarbon dates were converted to calendar years with the program CALIB v. 5.0.2 (Stuiver and Reimer, 1993). Calibration of wood material ages based on the atmospheric data of INTCAL98 (Stuiver et al., 1998b). Age calibration for the intact marine shell was based on MARINE98 (Stuiver et al., 1998a) using a regional marine reservoir correction of 790±25 (delta-R=390±25) years (Stuiver and Reimer, 1993). Calibrated ages presented as the median intercept. Age range represents the range having the greatest proportion under the 2-sigma curve.

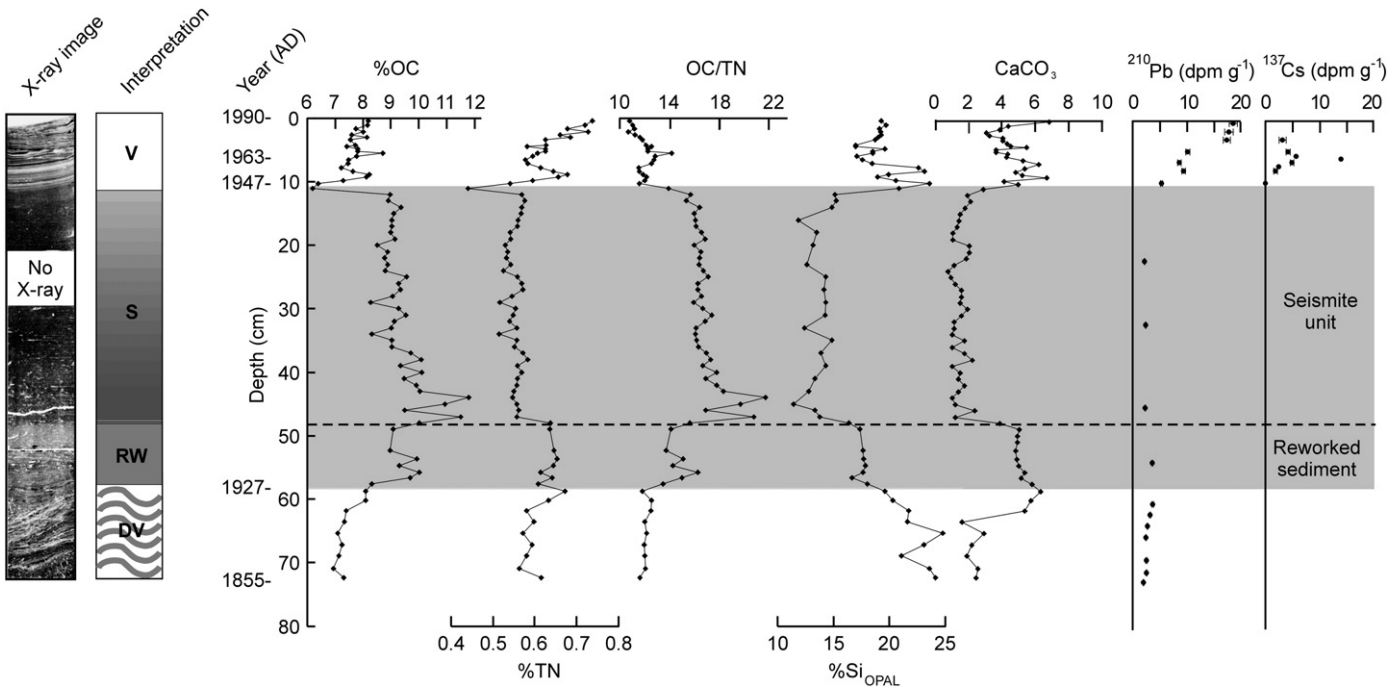

Fig. 3. Organic carbon (%OC), total nitrogen (%TN), organic carbon-total nitrogen (OC/TN), %opal, %$CaCO_3$, ^{210}Pb and ^{137}Cs values within the Soutar box core EFBC9703-2. A composite X-ray and schematic interpretation are presented showing varved sequences (V) overlying the seismite (S) unit, a reworked sediment unit (RW) and the basal unit of disturbed laminae (DV).

biomarkers (*Rhizosolenia setigera* - ca. AD 1940; *Minidiscus chilensis* - AD 1860) (Hay, 2005). Radiocarbon dates yielded a basal age of ca. AD 500. Diatom biomarker horizons (and sediment geochemistry discussed below) showed that the lowermost section of the ca. AD 1946 massive unit capped the top of the core. Two radiocarbon dates on small wood fragments recovered from a homogeneous mud unit yielded ages of AD 1555. The precise depth of these samples was uncertain as the 20-cm slab section used for extracting material for radiocarbon dating from this unit was disturbed during transport. These two radiocarbon ages appeared too "old" along the age-depth curve and most likely represented the deposition of re-worked wood material due to winnowing.

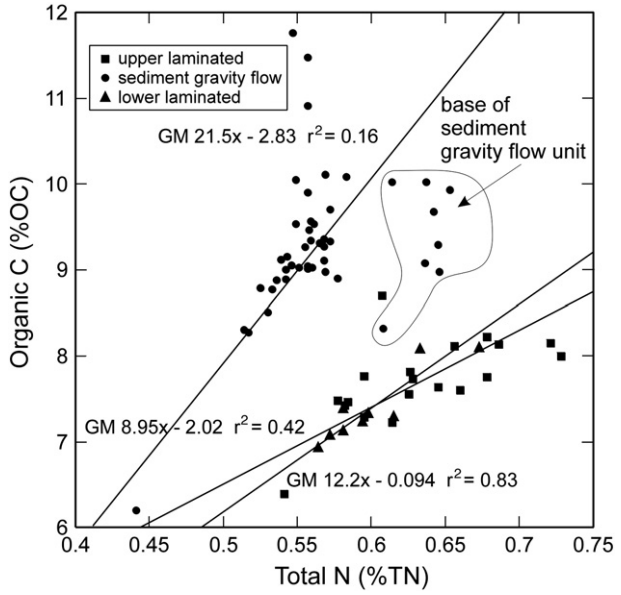

Fig. 4. Relationship between % organic C and % total N in core EFBC9703-2. Regressions are Model II or geometric mean regressions (Ricker, 1984). Slopes of these regressions provide an estimate of the mean organic C/N ratio of the sedimentary units. The sediment gravity flow unit regression includes the reworked sediments in spite of the markedly lower OC/TN ratios at the base of the unit.

4.2. Lithological description and geochemistry

4.2.1. Box core 9703-2 (ca. AD 1990–AD 1855)

The upper contact of the massive unit deposited ca. AD 1946 in this core has a sharp upper contact with the overlying deposits, whereas the bottom contact with the underlying sediments is indistinct, indicating disturbance of the underlying sediments during deposition of the unit and a rapid return to anoxic, quiescent conditions afterwards. Lead-210 and geochemical profiles show that the bottom portion of the unit is composed of reworked material and that minimal erosion of the underlying sequence occurred (Fig. 3).

Sediments in the upper laminated unit as well as the disturbed laminae at the base of the core had mean organic carbon (OC) contents

Table 2
Changes in major metal and trace element concentrations within a) the AD 1946 seismite relative to the over- and underlying sediments, and b) the homogeneous mud units relative to the varved sequences.

Element/Al	AD 1946 seismite	Homogeneous mud units
Ba	Decrease	No change
Cr	Increase	No change
Cu	Increase	No change
Fe	No change	Decrease
K	Decrease	No change
Mg	Increase	Decrease
Mn	Decrease	No change
Mo	Decrease	Decrease
Ni	No change	No change
Rb	Decrease	No change
$Si_{(non\text{-}bio)}$	No change	Decrease
Ti	Increase	Decrease
V	No change	No change
Zn	No change	No change
Zr	No change	Decrease

Differences between units were assessed using Mann-Whitney *U* tests, with a difference deemed significant when $p<0.05$.

of 7.61 ± 0.48%, total nitrogen (TN) values of 0.63 ± 0.05% and OC/TN ratios of 12.2 ± 0.67 (Fig. 3). In contrast, the massive unit (reworked sediment excepted) was characterized by significantly higher mean OC (at 9.31 ± 0.86%) and lower mean TN (0.57 ± 0.04) contents, resulting in a mean OC/TN ratio of 16.5 ± 1.5. OC content was highest towards the base of the unit. Regressions (Model II) of OC on TN (Fig. 4) show that the massive unit had a significant inorganic N content (i.e., 0.13% N at 0% OC), and that the organic C/N ratio (slope of the regression) was,

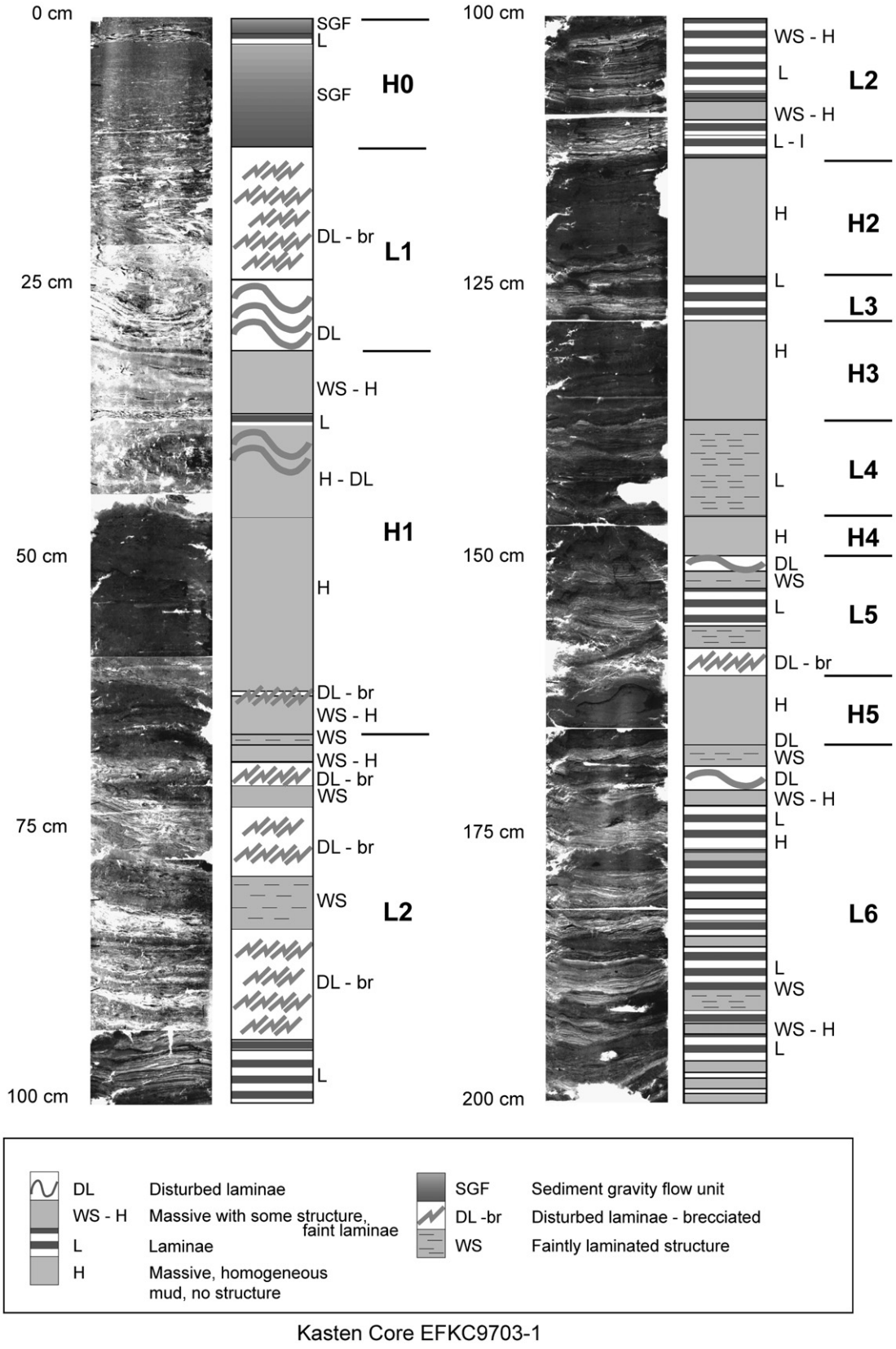

Fig. 5. Composite of X-ray images and interpretation of Kasten core EFKC9703-1.

on average, 21.5. In contrast, there was an insignificant amount of inorganic N in the laminated sections of the core (intercepts are either positive or are not significantly different from zero), confirming that the organic C/N ratio was, on average, 12.2 in the upper laminated section and 8.95 in the lower laminated section of core.

Calcium carbonate contents were significantly lower in the upper and middle sections of the massive unit compared with the over- and underlying laminated horizons (Fig. 3). This carbonate was almost entirely composed of comminuted shell debris. Mean opal concentrations were also lower ($15.0 \pm 2.2\%$) in the unit relative to the laminated horizons above and below this section ($19.4 \pm 1.8\%$ and $22.2 \pm 1.8\%$, respectively), but the values increased in the lower part of the unit, where OC values decreased. The lowest portion of the unit (50–57 cm depth) had higher $CaCO_3$ values. This contrast could be clearly seen by visual examination of the core (Fig. 3).

The massive unit was also distinguished from the laminated sections of the box core by the distribution of some of the major and minor elements (Table 2). In order to account for the dilution by biogenous components, all element data are ratioed to Al concentrations, hereafter referred to as normalized concentrations. Aluminium is a conservative tracer and has similar concentrations in a wide range of rock types (Calvert et al., 2001). Normalized Ti, Mg, Cr and Cu were higher (Mann-Whitney *U* test, all $p<0.05$) and normalized K, Mn, Ba, Rb, and Mo were lower ($p<0.05$) in the massive unit relative to the under- and overlying laminated units. Normalized Fe, V, Zn, Ni and Zr were not significantly ($p>0.05$) different in the two facies.

4.2.2. Kasten core 9703-1 (AD 1946–ca. AD 500)

The Kasten core (Fig. 5) contained five relatively thick (>5 cm) homogeneous mud units (H1 to H5) intercalated within predominantly laminated sections (L1 to L6). The lowermost, reworked section of the AD 1946 massive unit was denoted as unit H0. Homogeneous mud unit H1 was divided into two sub units (H1a, H1b) based on geochemical properties and diatom assemblages, discussed below. The unit contained two very thin laminated horizons, but we elected not to divide this section further.

As in the case of the box core, OC concentrations through the Kasten core were on average higher in the homogenous units ($8.15 \pm 0.57\%$) compared with the laminated sections ($7.4 \pm 0.65\%$), especially in the two thick units (H0 and H1b) at the top of the core (Fig. 6). This difference was significant at $p<0.001$ (Mann-Whitney *U* test). $CaCO_3$ content was highest in H0 and H1a. Carbonate values then decreased with depth through H1 and increased with depth in L2, after which there was a precipitous drop in values and a steady increase to another maximum at the base of L4 (Fig. 6). The carbonate content then again decreased abruptly, followed by another steady rise through L5 to the base of the core. The down-core increases in $CaCO_3$ occurred within the laminated sections with the thin homogeneous mud units not interrupting the down-core trends in carbonate concentration.

Overall, opal values were higher in the laminated ($23.7 \pm 3.4\%$) than the homogeneous mud ($20.4 \pm 2.8\%$) sections of the core and this difference was significant at $p<0.001$ (Fig. 6). However, opal values were distinctly higher in homogeneous mud units H0 and H1a compared with the super- and sub-adjacent laminated sections. Deeper in the core, this contrast was reversed, where laminated sections (especially L2, 3, 5 and 6) had higher opal contents than the adjacent homogeneous mud units.

OC/TN ratios were slightly, but non-significantly ($p<0.14$), different in the homogeneous mud (12.2 ± 0.95) and the laminated horizons (12.4 ± 0.82). Organic C/N ratios, deduced from the slopes of the regressions of OC on TN (Fig. 7) were, however, higher (13.5) in the laminated sections compared with the homogeneous mud units (8.65). These values translated into molar organic C/N ratios of 15.8 and 10.1, respectively. Note that the differences in C/N ratios in the two sediment lithologies in the Kasten core were *opposite* to the difference between the AD 1946 massive unit and the over- and underlying laminated sections in the box core.

Based on the organic properties, homogeneous mud unit H1 was sub-divided into two subunits. Unit H1a (34–50 cm) was distinct from the lower H1b unit (50–65 cm). Unit H1a had similar values to those of homogeneous mud units lower in the core, including less depleted $\delta^{13}C$ values, increased TN and OC, as well as reduced opal contents (Fig. 6).

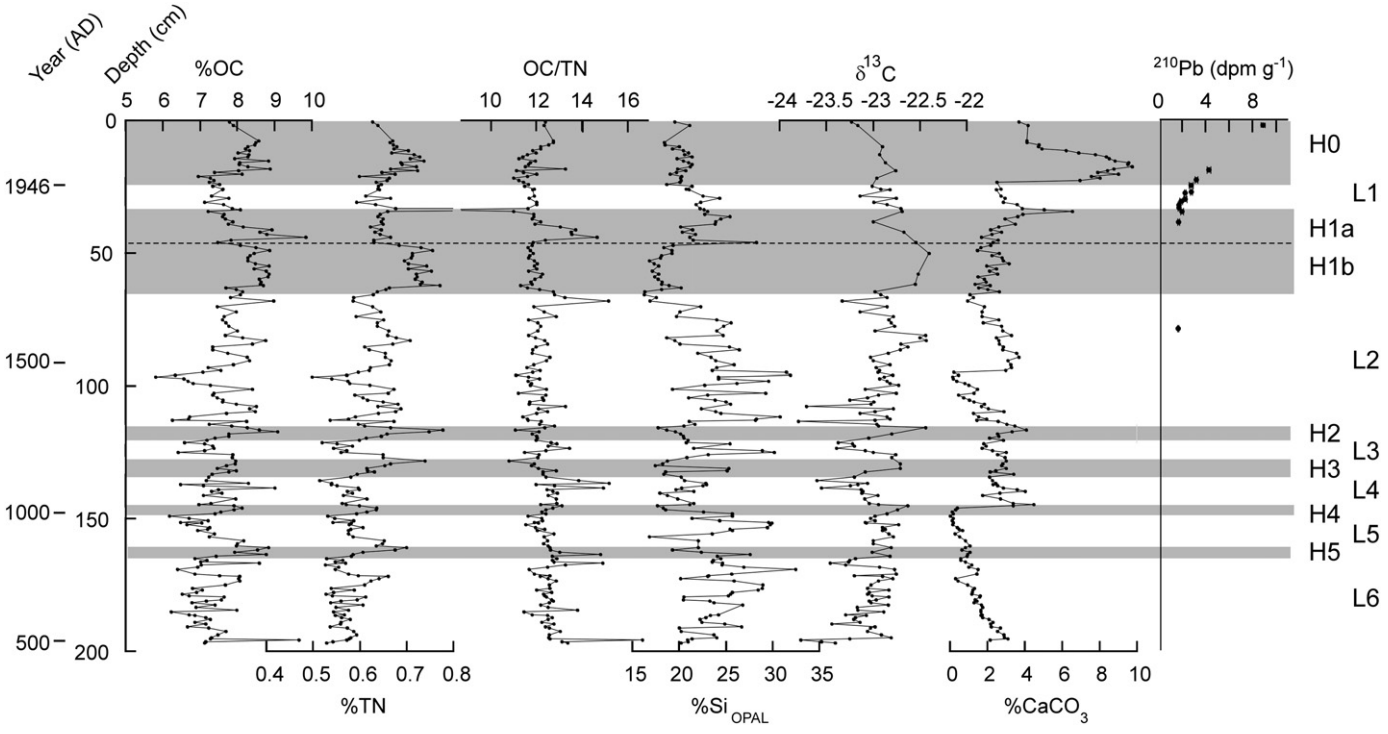

Fig. 6. Organic carbon (%OC), total nitrogen (%TN), OC/TN ratio, %opal, % $CaCO_3$, and ^{210}Pb values within the Kasten core EFKC9703-1. Grey zones indicate relatively thick (>5 cm) homogeneous mud units (H) intercalated with predominantly laminated (L) units.

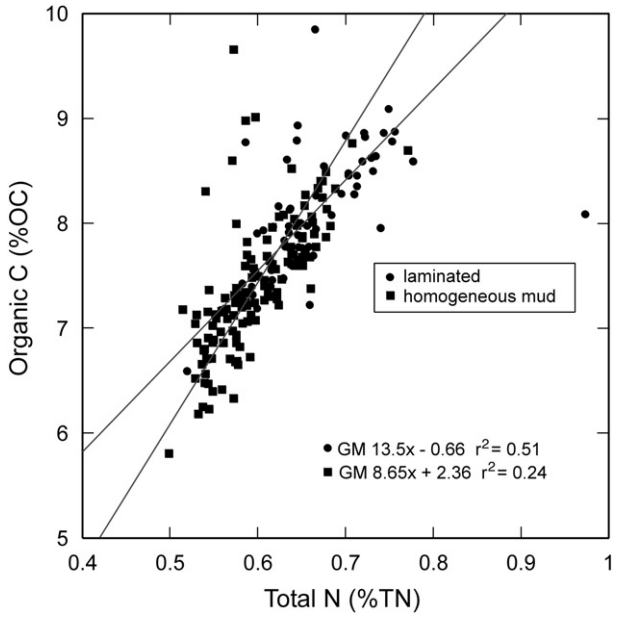

Fig. 7. Regression of OC on TN for the combined laminated and homogeneous mud sections of core 9703-1. Regressions are Model II or geometric mean regressions (Ricker, 1984).

Values of opal, TN, and OC decreased within H1a with an important exception between 40 and 46 cm where OC and OC/TN values peaked, matched by a reduction in opal. Carbon isotope values were only slightly more depleted within H1a.

Combining the data for all homogeneous mud and all laminated units (Table 2), there was little difference between the two facies in normalized K, Ba, Ni, Mn, Zn, Rb, V, Cu, Cr (all Mann-Whitney *U* tests $p>0.17$), whereas the homogeneous mud sections had lower normalized $Si_{(non\text{-}bio)}$, Ti, Fe, Zr, Mo and Mg (all Mann-Whitney *U* tests $p<0.05$).

As in the case of the box core, molybdenum concentrations were substantially higher (Mann-Whitney *U* test $p<0.001$) than average shale abundances (Wedepohl, 1971) in both the laminated and homogeneous mud sections of the Kasten core. Molybdenum concentrations were lower in H1–H5 than in the over- and underlying laminated sections, but they were still elevated compared to oxygenated sediment values (Appendix Fig. 4).

4.3. Fossil diatom assemblages

Diatom assemblages within the Kasten core were dominated by the lightly silicified *Skeletonema costatum*, with *Chaetoceros* spp. (mostly resting spores), *Thalassiosira* spp. and *Cyclotella choctawhatcheeana* (Fig. 8). Diatoms associated with the spring-summer blooms in British Columbia coastal regions (e.g., *S. costatum*, *Thalassiosira. nordenskioeldii*, *T. pacifica*, and *Chaetoceros* spp.) were most abundant within the laminated units. Total diatom valve and resting spore abundances were highly correlated with % opal (Pearson correlation, $p<0.001$).

Cyclotella choctawhatcheeana showed maxima when opal and *S. costatum* were at minimal levels (Fig. 8). Peak relative and absolute abundances of *C. choctawhatcheeana* were associated with the thick homogeneous mud units as well as thin (<2 cm) homogeneous mud units (for example a peak at 75–77 cm depth). Pair-wise correlation of the absolute abundance of *C. choctawhatcheeana* with opal, as well as the typical spring-summer bloom taxa of *S. costatum*, *T. nordenskioeldii*, and *Chaetoceros* spp. was significantly negative ($p<0.001$).

Within the homogeneous mud units, *Actinoptychus senarius*, *Odontella longicruris* and *Coscinodiscus radiatus* generally increased in abundance whereas *Paralia sulcata* occasionally had peak abundance within these sequences (Fig. 8). A summed record of oligohaline planktonic diatom abundance showed little relationship to the homogeneous mud units.

As observed with the organic properties, the fossil diatom assemblages of units H1a and H1b were dissimilar. Diatom assemblages within H1b were similar to other homogeneous mud units, marked by an increased abundance of *C. choctawhatcheeana* and a reduced abundance of *S. costatum*, *Thalassiosira* spp., and *Chaetoceros* spp. On the other hand, diatom assemblages within the upper sub-unit (H1a) were more consistent with laminated sequences, a typical spring-summer bloom succession indicating greater production (Fig. 8). *Coscinodiscus radiatus*

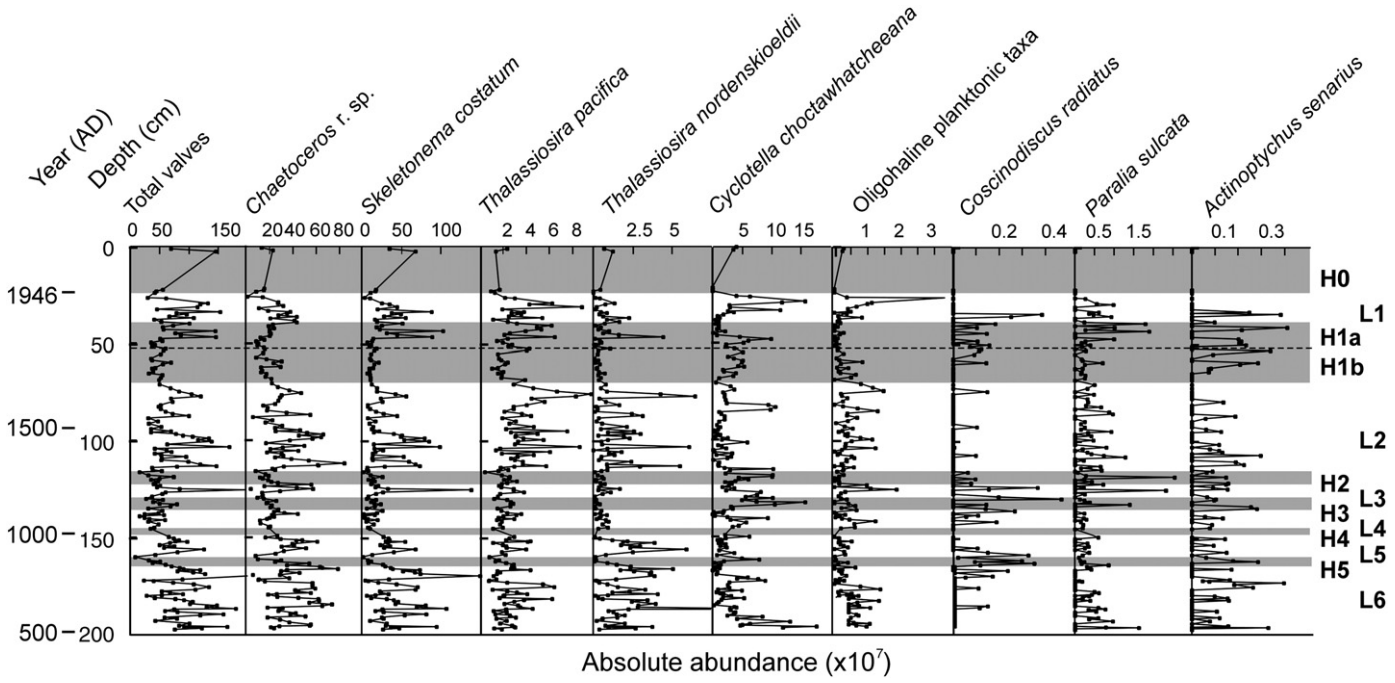

Fig. 8. Absolute abundance (valves $x10^7$) for selected diatom taxa within Kasten core EFKC9703-1. Grey zones indicate relatively thick (>5 cm) homogeneous mud units (H) intercalated with predominantly laminated (L) units.

and *Actinoptychus senarius* showed a more consistent abundance in the lower H1b unit relative to unit H1a.

5. Discussion

5.1. Origin of the AD 1946 massive unit

Varve counts and the ^{137}Cs peak support the interpretation of Dallimore et al. (2005) that this massive unit represents a seismite resulting from the M_w ~ 7.2 earthquake of June 23, 1946 that affected central Vancouver Island. This seismic event produced numerous aerial and sub-aerial slope failures in the region (Rogers and Hasewaga, 1978; Rogers, 1980). The geochemical signal of the seismite deposit reflects the movement of terrestrial material from the relatively shallow fjord sides to the fjord bottom. Within the seismite, reduced ^{210}Pb values relative to overlying and underlying sediments attest to a movement and re-deposition of older sediments at the bottom of the inner fjord. Peak OC values near the base of this unit (11–12%) and elevated organic C/N values throughout the interval represent the deposition of terrestrial organic material transported from the littoral areas, which contain vascular plant debris and soil-derived organic materials with lower N content (Meyers, 1997). The presence of plant fragments (i.e., leaves, needles, and twigs) within this unit was observed upon recovery of a short freeze core TUL99B04 from the inner basin (Dallimore et al., 2005), supporting this interpretation.

Major and minor element data reflect both the poorly sorted nature of the deposit and the change in source material relative to the laminated sediment horizons. Normalized Ba, Rb, although they have different values in the two sediment facies, are also largely coherent with the variations in normalized Cu, Ni, V, Zn, Cr and Zr (Appendix Figs. 1 and 2). This suggests that there is considerable heterogeneity in the composition of the laminated and the gravity flow sediment in the box core and this is manifested by the intercalation of sediments of different mineralogy and/or grain size, possibly from different sources. Normalized Si, Ti, and Zr have been used as sediment grain size proxies in marine sediments (Calvert et al., 2001; Ivanochko et al., 2008). In an analysis of silt-sand-clay fractions, Ivanochko et al. (2008) confirmed that higher Si/Al, Ti/Al, and Zr/Al values within sediments recovered from Effingham Inlet are marked by an increase in grain size. A decrease in opal within the unit reflects the transport of opal-poor material from shallower depths where fossil diatom concentrations are reduced (Hay et al., 2003). Molybdenum concentrations are significantly higher than average shale abundances (Wedepohl, 1971) in both laminated horizons and the seismite unit, although the Mo/Al ratio is lower in the upper three quarters of the latter. The levels of Mo enrichment demonstrate that both lithologies formed under bottom water anoxia, suggesting the material for this seismite unit possibly originated from a submarine slope failure at a depth of greater than 45 m (depth of the inner basin sill).

5.2. Origin of the homogeneous mud units

In contrast to the terrestrial influence within the AD 1946 seismite, the homogeneous mud units in the longer Kasten core are composed of material having a stronger marine signature relative to the over- and underlying laminated units. Accepting the difference in C/N ratios between marine and terrestrial OM (Emerson and Hedges, 1988) implies that the homogeneous mud facies in the Kasten core contained more planktonic OM than the laminated units. This is corroborated by the heavier organic carbon δ^{13}C values (significant at $p<0.001$) in the homogeneous mud sediments (Fig. 6), which are typical of marine OM (Deines, 1980).

The δ^{13}C values for phytoplankton along the British Columbia and Washington State coasts have been estimated at −19.5 to −22.0‰ (Hedges et al., 1988; Prahl et al., 1994). Timothy et al. (2003) estimated marine end-member δ^{13}C values of −16.7‰ for Saanich Inlet on southern Vancouver Island and −18.8‰ for Jervis Inlet on the British Columbia mainland.

The δ^{13}C value for terrestrial organic matter is currently unknown for the Effingham Inlet watershed. However, soils around Jervis Inlet, a fjord that lies within the same coastal western hemlock (CWH) biogeoclimatic zone (Meidinger and Pojar, 1991) as Effingham Inlet, were slightly lighter at −26.5‰ (Timothy et al., 2003). We discount any influence of C_4 vegetation in the watershed of the inlet, which could impose a heavier isotopic signal on the sedimentary OM, because vegetation around Effingham Inlet is dominated by C_3 vegetation and C_4 grasses are rare in the coastal Washington-British Columbia region (Teeri and Stowe, 1976).

The elemental data show that, despite the considerable heterogeneity, there were differences in the chemical and mineralogical composition of the laminated and homogeneous mud units in the Kasten core. The heterogeneity is related, in part, to variability within the laminated (L) units. Although predominantly laminated, these units also contain thin (<2 cm) homogeneous mud and weakly laminated layers where distinct laminae are absent. The variability observed in these elemental ratios is remarkably coherent, many of the maxima and minima being defined by several data points (Appendix Figs. 3 and 4). Normalized Ti, K, Mg, Cu and Cr are lower or show little change in the homogeneous mud units in comparison with the over- and underlying laminated units (Table 2). This is in contrast to the AD 1946 seismite where concentrations of these elements are higher relative to the laminated units. Normalized $Si_{(non\text{-}bio)}$ and Zr being higher on average in the laminated units ($p<0.069$ and 0.001, respectively), suggests that these sediments are coarser-grained. Sharp maxima in Zr/Al in both sediment facies are matched by maxima in normalized Ti, Fe, Mn, K and Rb, indicating the probable presence of thin silt or sand layers in otherwise muddy material (Appendix Figs. 3 and 4).

Laminated units on average have higher opal contents, higher organic C/N ratios, lighter δ^{13}OC values and higher normalized $Si_{non\text{-}bio}$, Ti, Fe, Mg, Zr, Ba, Ni and Mo than the homogeneous mud units, which in turn have higher organic C and $CaCO_3$ concentrations. Concentrations of Mo within the homogeneous mud sections of the core clearly show that they were formed under bottom water anoxia, although the degree of anoxia or the sedimentation rate of the disturbed or reworked types of homogeneous mud units is probably different from that prevailing during the accumulation of the laminated sections.

Taken together, our geochemical data clearly demonstrate that the source material of the AD 1946 seismite was distinct from that of the homogeneous mud units:

- Within the AD 1946 seismite, organic properties demonstrate a strong terrestrial influence whereas within the homogeneous mud units, these geochemical proxies coupled with the heavier δ^{13}C values demonstrate a strong marine influence.
- Trace element concentrations show that the seismite and homogeneous mud units have different aluminosilicate mineralogy, with the latter facies deposited under less intense (less sulphidic) bottom water anoxia than over- and underlying laminated sequences.

5.3. Environmental control of homogeneous mud unit formation

5.3.1. Surface water conditions

Deposition of the homogeneous units occurred during surface water conditions that favored the brackish taxon *C. choctawhatcheeana* and caused suppression of the typical *Thalassiosira-Skeletonema-Chaetoceros* spring bloom succession. *C. choctawhatcheeana* (often referred to as *C. caspia* (Sancetta, 1989, 1990; Fourtanier and Barron, 2000) in Saanich Inlet; and *C. hakanssoniae* in the Baltic Sea (Håkansson et al., 1993; Carvalho et al., 1995)) is an estuarine taxon that occurs in brackish waters having a salinity <22 (Prasad et al., 1990; Håkansson et al., 1993; Carvalho et al., 1995; Ryves et al., 2004). Sancetta (1989) observed that *C. choctawhatcheeana* (as *C. caspia*) was dominant in the summer flora

within Jervis Inlet during a year having a weak spring bloom due to reduced salinity and high turbidity in the surface waters.

The limited bloom of marine taxa and dominance of *C. choctawhatcheeana* would require either increased precipitation or increased snowmelt runoff during the spring and summer months. The significant negative correlation between *C. choctawhatcheeana* and the dominant spring bloom taxa also suggests that environmental conditions must have persisted for an extended period of time, ruling out the possibility of a single, brief and intense spring or summer rainfall event.

At present, peak rainfall occurs during the months of October through February. Present-day snowfall accumulation is limited in the watershed thereby reducing the spring melt freshet. Increased runoff forcing the suppression of the spring bloom would require an increase in winter snowfall as well as cooler winter conditions favoring greater snow accumulation than at present. Alternatively, sunlight could have been limited with increased spring precipitation and increased river discharge thereby suppressing the typical spring bloom. Regardless of the exact process creating more brackish surface conditions, there is a clear link between climate and oceanographic processes in the fjord. These conditions have not been observed in Effingham Inlet since the middle 20th century as evidenced by the strongly laminated sediments and absence of *C. choctawhatcheeana* in the sediment record above the AD 1946 seismite (Hay, 2005).

It could be expected that increased runoff, via snowmelt and/or precipitation, into Effingham Inlet would be coupled with an increased occurrence of freshwater (oligohaline) planktonic diatom taxa and possibly more euryhaline benthic taxa within the homogeneous mud units. However, the diatom record is ambiguous, providing no clear freshwater signal. Hay et al. (2003) have shown that, due to the limited surface currents in the spring and summer, any increase in freshwater diatoms is mainly restricted to the upper portion of the inner basin and that this signal would be minor and difficult to discern. Furthermore, in nearby Saanich Inlet, most benthic and freshwater taxa are deposited during the winter months (Sancetta, 1989; McQuoid and Hobson, 1997) rather than showing an association with spring/summer precipitation patterns.

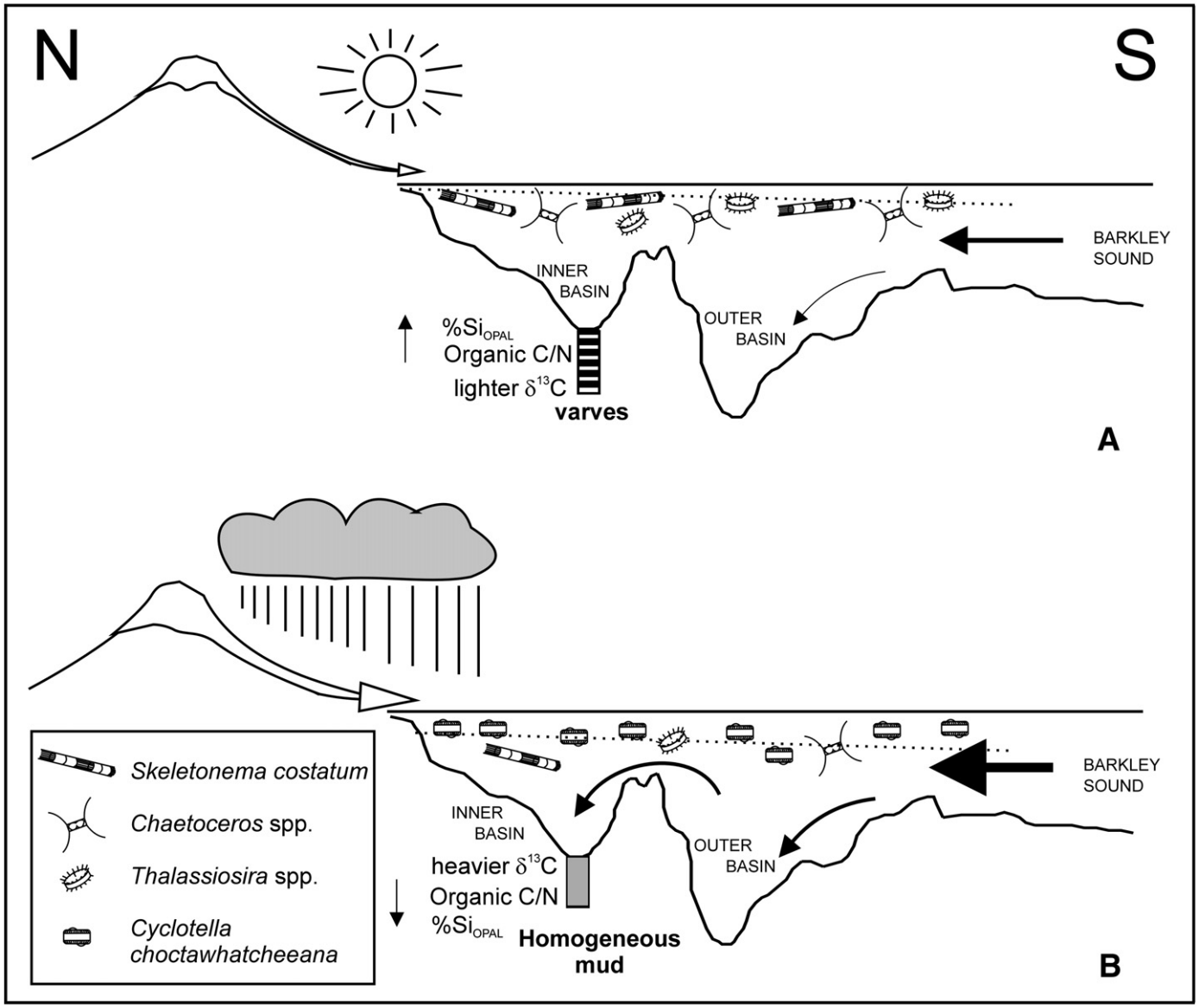

Fig. 9. Summary diagram of processes and sediment signatures related to the deposition of (A) varved units and (B) homogeneous mud units in Effingham Inlet. In A, a reduced snowpack and favorable spring-summer conditions limit freshwater input into the fjord and deep water renewal is weak. In B, a thick snowpack and/or increased spring-summer cloudiness suppress the spring-summer diatom production while increased stratification of the water column favors an intensified estuarine circulation and increased bottom water renewal (symbol - downarrow)- er = lower; (symbol - uparrow) er = higher.

5.3.2. Bottom water renewal events and deposition

The intrusion of bottom waters and the deposition of sediment from outside the fjord has been suggested to account for the late Holocene sedimentary patterns recorded in cores from the inner and outer basins of Effingham Inlet (Dallimore et al., 2005). The movement of bottom waters across sills into the deep basins or at intermediate depths in the water column often results in increased sediment flux at depth due to re-suspension of sediment and transport of material from outside the fjord (Timothy et al., 2003). One of the principal environmental conditions suggested to facilitate bottom water renewal in fjords along the west coast of Vancouver Island is an increased stability of the upper water column (Dallimore et al., 2005).

Diatom assemblages within the homogeneous mud units show that a reduced surface salinity creates the necessary conditions for bottom water renewal. The presence of a relatively thick freshwater-brackish water lens along the surface within the inner basins of Effingham Inlet would produce a more stratified upper water column. This stability facilitates bottom water renewal resulting in the transport of sediment across the sill separating the inner and outer basins and deposition of homogeneous mud units (Fig. 9). Bottom water renewal in the inner basin is enhanced by the gradual reduction in density of near-bottom waters by diffusion and mixing processes (Thomson, 1994; Pawlowicz et al., 2007).

Bottom water renewal can provoke the re-suspension and reworking of sediments by bottom currents, causing mixing of previously laminated sequences and deposition of homogeneous mud units. Furthermore, material from Barkley Sound and/or the outer portion of the fjord is transported into the inner basin during these events. Geochemical properties (lower organic OC/N and more isotopically heavy $\delta^{13}C$ values) reflect the introduction of this predominantly marine material. Diatom assemblages support this hypothesis, as peaks of diatom taxa associated with sediments of the outer fjord and Barkley Sound including *Actinoptychus senarius*, *Coscinodiscus radiatus* and *Paralia sulcata* (Hay et al., 2003) are often found within the homogeneous mud deposits.

The geochemical and microbiological composition of unit H1 suggests this unit reflects a mixture of depositional conditions. Unit H1b possibly reflects an extended period of frequent bottom water renewal coupled with reduced surface salinity conditions, analogous to other homogeneous mud units found within the sediment record. The upper unit, H1a, on the other hand, suggests a change in environmental conditions that favored typical *Skeletonema-Thalassiosira-Chaetoceros* spring and summer blooms and higher surface salinities. At the same time, however, the processes of bottom water renewal and sediment re-suspension (and temporarily oxygenated conditions) continued. Thus, during this period, surface stability (as occurs during brackish surface water conditions) was not the determining condition for bottom water renewal in Effingham Inlet.

Based on sedimentary evidence for the AD 1946 earthquake deposit, we also expected to find evidence for a seismite related to the major (M_w~9) earthquake and tsunami of January 27, 1700 (Satake et al., 1996) in the cores recovered from Effingham Inlet. Evidence for the severity of this seismic event is well documented for the region (e.g. Jacoby et al., 1997; Clague et al., 1999; Blais-Stevens and Clague, 2001). Based on the ^{14}C chronology of the Kasten core as well as the lithological, geochemical, and microfossil record, a possible seismite related to this event occurs at 40–46 cm depth. This 6 cm-thick deposit is marked by an increase in OC/TN values, pointing to an increased influence of terrestrial material. The H1 unit also overlies disturbed and brecciated sediments, similar to those underlying the AD 1946 seismite and other seismites identified from Saanich Inlet (Blais-Stevens and Clague, 2001). However, the patterns of major and minor element variability in this section of the core did not match those of the AD 1946 sediment gravity flow unit, nor were there any distinct changes in their values relative to the sediments lying immediately above and below. Opal decreases, but not to minimal values, such as observed in the AD 1946 seismite, and values for $\delta^{13}C$ do not record a major change, although only a single sample was recovered from this section of the core.

In contrast to the AD 1946 event, this unit appears to have been deposited during a period of frequent bottom water renewal. It is likely that the original signature has been diluted due to re-suspension and reworking of the sediment. It is also apparent that, if present, this seismite unit is thinner than the AD 1946 seismite despite the severity of the AD 1700 seismic event. On-going work involving the recovery of additional short cores from northern British Columbia fjords should reveal if a regional and distinct AD 1700 seismite is preserved within the coastal sediments of British Columbia.

In summary, the formation of most homogenous mud units in Effingham Inlet appears to be controlled by environmental conditions:

- Diatom assemblages within the homogeneous mud units suggest that deposition occurred during brackish surface water conditions, related to an increase in snowmelt or precipitation runoff at the head of the fjord.
- These environmental conditions increased upper water column stability thereby favoring bottom water intrusions into the silled basins of the inlet. These bottom currents were responsible for the re-suspension of sediments and advection of material into the inner basin.
- Although expected, a distinct seismite related to the AD 1700 earthquake was not observed, likely due to reworking of the deposit by subsequent bottom water renewal events during this period.

6. Conclusions

Detailed geochemical, isotopic, and diatom analyses of a 1500-year sediment record from the inner basin of Effingham Inlet show that homogeneous mud units that interrupt the laminated sequences throughout the sediment record are related to intermittent bottom water renewal events, which caused re-suspension of previously deposited material and a flux of imported sediments to the inner basin. These deposits have a marine geochemical signal that is distinct from the terrestrial influence identified within the AD 1946 seismite. Diatom assemblages in these homogeneous mud units show that bottom water renewal events in Effingham Inlet are associated with more brackish surface conditions, which lead to increased stratification of the upper water column. The homogeneous mud units therefore represent indicators of particular paleoenvironmental conditions in Effingham Inlet. Analysis of their occurrence and their timing relative to regional paleoenvironmental and paleoclimatic conditions will provide a better understanding of oceanographic and climatic variability within the fjord over the Late Holocene. Utilization of geochemical properties coupled with fossil diatom assemblages within the sedimentary sequence has allowed for accurate determination of both the source and the mechanism responsible for the deposition of such units.

Acknowledgements

This paper forms a contribution to the Natural Sciences and Engineering Research Council (NSERC) funded project “Long-term variability in pelagic fish abundance and oceanographic conditions on the British Columbia Shelf: implications for strategic fisheries planning”. The core recovery operation was part of a National Sea Grant College Program of NOAA, under project R/CZ-112A of the California Sea Grant System. MBH was funded by “Fonds pour la Formation de Chercheurs et l'aide à la Recherche” (FCAR-Québec) and “La Fondation de l'Université Laval”, and NSERC funding supported the geochemical analyses at UBC. We are very grateful to Vicente Ferreira-Bartrina and Hector Lozano (Centro de Investigación Científica y Educación Superior de Ensenada (CICESE), Ensenada, Mexico) who were responsible for slabbing and sectioning the box and Kasten core

material. Logistical support from the Centre d'études nordiques (CEN, Université Laval) is appreciated and we thank the crew of the *C.S.S. John P. Tully* and technical staff of the Institute of Ocean Sciences (Sidney, British Columbia). We thank the members of the Aquatic Paleoecology Laboratory at Université Laval, as well as Tim Patterson, Antoon Kuijpers, and the anonymous reviewers who provided helpful comments on an earlier version of this manuscript.

Appendix A. Supplementary data

Supplementary data associated with this article can be found, in the online version, at doi:10.1016/j.margeo.2009.03.004.

References

Binford, M.W., 1990. Calculation and uncertainty analysis of 210Pb dates for PIRLA project lake sediment cores. J. Paleolimnol. 3, 253–267.
Blais-Stevens, A., Clague, J.J., 2001. Paleoseismic signature in late Holocene sediment cores from Saanich Inlet, British Columbia. Mar. Geol. 175, 131–148.
Blais-Stevens, A., Clague, J.J., Bobrowsky, P.T., Patterson, R.T., 1997. Late Holocene sedimentation in Saanich Inlet, British Columbia, and its paleoseismic implications. Can. J. Earth Sci. 34, 1345–1357.
Calvert, S.E., Pedersen, T.F., Karlin, R.E., 2001. Geochemical and isotopic evidence for post-glacial palaeoceanographic changes in Saanich Inlet, British Columbia. Mar. Geol. 174, 287–305.
Carvalho, L.R., Cox, E.J., Fritz, S.C., Juggins, S., Sims, P.A., Gasse, F., Battarbee, R.W., 1995. Standardizing the taxonomy of saline lake *Cyclotella* spp. Diatom Res. 10, 229–240.
Chang, A.S. 2004. Ultra-high resolution sediment analysis and diatom paleoecology from Effingham Inlet, British Columbia, Canada: Implications for late Holocene environmental change. Unpublished Ph.D. thesis, Carleton University, Ottawa.
Chang, A.S., Patterson, R.T., McNeely, R., 2003. Seasonal sediment and diatom record from late Holocene laminated sediments, Effingham Inlet, British Columbia, Canada. Palaios 18, 477–494.
Clague, J.J., Hutchinson, I., Mathewes, R.W., Patterson, R.T., 1999. Evidence for Late Holocene tsunamis at Catala Lake, British Columbia. J. Coast. Res. 15, 45–60.
Dallimore, A., Thomson, R.E., Bertram, M.A., 2005. Modern to Late Holocene deposition in an anoxic fjord on the west coast of Canada: implications for regional oceanography, climate and paleoseismic history. Mar. Geol. 219, 47–69.
Dallimore, A., Enkin, R.J., Pienitz, R., Southon, J.R., Baker, J., Wright, C.A., Pedersen, T.F., Calvert, S.E., Ivanochko, T., Thomson, R.E., 2009. Postglacial evolution of a Pacific coastal fjord in British Columbia, Canada: interactions of sea-level change, crustal response, and environmental fluctuations - results from MONA core MD02-2494. Can. J. Earth. Sci. 45, 1345–1362.
Deines, P., 1980. The isotopic composition of reduced carbon. In: Fritz, P., Fontes, J.C. (Eds.), Handbook of Environmental Isotope Geochemistry. Elsevier, Amsterdam, pp. 329–406.
Emerson, S., Hedges, J.I., 1988. Processes controlling the organic carbon content of open ocean sediments. Paleoceanography 3, 621–634.
Fourtanier, E., Barron, J.A., 2000. Data Report: Intra-annual variability of the diatom assemblages at Hole 1034B (Saanich Inlet) near 9 ka. In: Bornhold, B.D., Firth, J.V. (Eds.), Proceedings of the Ocean Drilling Program, Ocean Drilling Program. College Station, Texas, pp. 3–10.
Håkansson, H., Hajdu, S., Snoeijs, P., Loginova, L., 1993. *Cyclotella hakanssoniae* Wendker and its relationship to *C. caspia* Grunow and other similar brackish water *Cyclotella* species. Diatom Res. 8, 333–347.
Hay, M.B. 2005. Reconstitution des conditions océanographiques et climatiques de l'holocène supérieur à Effingham Inlet, île de Vancouver, Colombie Britannique, Unpublished Ph.D. thesis, Université Laval, Québec, (In English and French), 304 p. http://www.theses.ulaval.ca/auteurs.html.
Hay, M.B., Pienitz, R., Thomson, R.E., 2003. Distribution of diatom surface sediment assemblages within Effingham Inlet, a temperate fjord on the west coast of Vancouver Island (Canada). Mar. Micropaleontol. 48, 291–320.
Hay, M.B., Dallimore, A., Thomson, R.E., Calvert, S.E., Pienitz, R., 2007. Diatom record of late Holocene oceanography and climate along the west coast of Vancouver Island, British Columbia (Canada). Quat. Res. 67, 33–49.
Hedges, J.I., Clark, W.A., Cowie, G.L., 1988. Organic matter sources to the water column and surficial sediments of a marine bay. Limnol. Oceanogr. 33, 1116–1136.
Ivanochko, T.S., Calvert, S.E., Southon, J.R., Enkin, R.J., Baker, J., Dallimore, A., Pedersen, T.F., 2008. Determining the post-glacial evolution of a northeast Pacific coastal fjord using a multiproxy geochemical approach. Can. J. Earth Sci. 45, 1331–1344.
Jacoby, G.C., Bunker, D.E., Benson, B.E., 1997. Tree-ring evidence for the AD 1700 Cascadia earthquake in Washington and northern Oregon. Geology 25, 999–1002.
Jensen, K.G., Kuijpers, A., Koç, N., Heinemeier, J., 2004. Diatom evidence of hydrographic changes and ice conditions in Igaliku Fjord, south Greenland, during the past 1500 years. Holocene 14, 152–164.
Kogler, F.-C., 1963. Das Kastenlot. Meyniana 13, 1–7.
McFarlane, G.A., Ware, D.M., Thomson, R.E., Mackas, D.L., Robinson, C.L.K., 1997. Physical, biological and fisheries oceanography of a large ecosystem (west coast of Vancouver Island) and implications for management. Oceanol. Acta 20, 191–200.
McMinn, A., Heijnis, H., Harle, K., McOrist, G., 2001. Late-Holocene climatic change recorded in sediment cores from Ellis Fjord, eastern Antarctica. Holocene 11, 291–300.
McQuoid, M.R., Hobson, L.A., 1997. A 91-year record of seasonal and interannual variability of diatoms from laminated sediments in Saanich Inlet, British Columbia. J. Plank. Res. 19, 173–194.
Meidinger, D., Pojar, J., 1991. Ecosystems of British Columbia. Research Branch. Ministry of Forests, Victoria, British Columbia.
Meyers, P.A., 1997. Organic geochemical proxies of paleoceanographic, paleolimnologic, and paleoclimatic processes. Org. Geochem. 27, 213–250.
Mortlock, R.A., Froelich, P.N., 1989. A simple method for the rapid determination of biogenic opal in pelagic marine sediments. Deep-Sea Res. 36, 1415–1426.
Patterson, R.T., Guilbault, J.-P., Thomson, R.E., 2000. Oxygen level control on foraminiferal distribution in Effingham Inlet, Vancouver Island, British Columbia. J. Foraminiferal Res. 30, 321–335.
Pawlowicz, R., Riche, O., Halverson, M., 2007. The circulation and residence time of the Strait of Georgia using a simple mixing-box approach. Atmosphere-Ocean 45 (4), 173–193.
Pickard, G.L., 1963. Oceanographic characteristics of inlets of Vancouver Island, British Columbia. J. Fish. Res. Board Can. 20, 1109–1144.
Prahl, F.G., Ertel, J.R., Goñi, M.A., Sparrow, M.A., Eversmeyer, B., 1994. Terrestrial organic carbon contributions to sediments on the Washington margin. Geochim. Cosmochim. Acta 58, 3035–3048.
Prasad, A.K.S.K., Nienow, J.A., Livingston, R.J., 1990. The genus *Cyclotella* (Bacillariophyta) in Choctawhatchee Bay, Florida, with special reference to *C. striata* and *C. choctawhatcheeana* sp. nov. Phycol. 29, 418–436.
Ricker, W.E., 1984. Computation and uses of central trend lines. Can. J. Zool. 62, 1897–1905.
Rogers, G.C., 1980. A documentation of soil failure during the British Columbia earthquake of 23 June, 1946. Can. Geotech. J. 17, 122–127.
Rogers, G.C., Hasewaga, H.S., 1978. A second look at the British Columbia earthquake of June 23, 1946. Bull. Seismol. Soc. Am. 68, 653–675.
Ryves, D.B., Clarke, A.L., Appleby, P.G., Amsinck, S.L., Jeppesen, E., Landkildehus, F., Anderson, N.J., 2004. Reconstructing the salinity and environment of the Limfjord and Vejlerne Nature Reserve, Denmark, using a diatom model for brackish lakes and fjords. Can. J. Fish Aquat. Sci. 61, 1988–2006.
Sancetta, C., 1989. Spatial and temporal trends of diatom flux in British Columbian fjords. J. Plankton Res. 11, 503–520.
Sancetta, C., 1990. Occurrence of Thalassiosiraceae (Bacillariophyceae) in two fjords of British Columbia. Beih. Nova Hedwigia 100, 199–215.
Satake, K., Shimazaki, K., Tsuji, Y., Ueda, K., 1996. Time and size of a giant earthquake in Cascadia inferred from Japanese tsunami records of January 1700. Nature 378, 246–249.
Schrader, H.J., Gersonde, R., 1978. Diatoms and silicoflagellates. Utrecht Micropaleont. Bull. 17, 129–176.
Stronach, J.A., Ng, M.K., Foreman, M.G., Murty, T.S., 1993. Tides and currents in Barkley Sound and Alberni Inlet. Mar. Geod. 16, 1–41.
Stuiver, M., Reimer, P.J., 1993. Extended 14C database and revised CALIB radiocarbon calibration program. Radiocarbon 35, 215–230.
Stuiver, M., Reimer, P.J., Bard, E., Beck, J.W., Burr, G.S., Hughen, K.A., Kromer, B., McCormac, F.G., Plicht, J., Spurk, M., 1998a. INTCAL98 Radiocarbon age calibration 24,000–0 cal BP. Radiocarbon 40, 1041–1083.
Stuiver, M., Reimer, P.J., Brazunias, T.F., 1998b. High-precision radiocarbon age calibration for terrestrial and marine samples. Radiocarbon 40, 1127–1151.
Syvitski, J.P.M., Shaw, J., 1995. Sedimentology and geomorphology of fjords. In: Perillo, G.M.E. (Ed.), Geomorphology and sedimentology of estuaries. Developments in Sedimentology, vol. 53. Elsevier Science, pp. 113–178.
Teeri, J.A., Stowe, L.G., 1976. Climate patterns and the distribution of C4 grasses in North America. Oecol. 23, 1–12.
Thomson, R.E., 1994. Physical oceanography of the Strait of Georgia-Puget Sound-Juan de Fuca Strait System. In: Wilson, R., Beamish, R., Aitkens, F., Bell, J. (Eds.), Review of the marine environment and biota of Strait of Georgia, Puget Sound and Juan de Fuca Strait. Can. Tech. Report of Fish. Aquat. Sci., vol. 1948, pp. 36–100.
Thomson, R.E., Hickey, B.M., LeBlond, P.H., 1989. The Vancouver Island Coastal Current: fisheries barrier and conduit. In: Beamish, R.J., McFarlane, G.A. (Eds.), Effects of ocean variability on recruitment and an evaluation of parameters used in stock assessment models. Can. Spec. Pub. Fish. Aquat. Sci., vol. 108, pp. 265–296.
Timothy, D.A., Soon, M.Y.S., Calvert, S.E., 2003. Settling fluxes in Saanich and Jervis Inlets, British Columbia, Canada: sources and seasonal patterns. Prog. Oceanogr. 59, 31–73.
Wedepohl, K.H., 1971. Environmental influences on the chemical composition of shales and clays. In: Ahrens, L.H., Press, F., Runcorn, S.K., Urey, H.C. (Eds.), Physics and Chemistry of the Earth. Pergamon, Oxford, pp. 307–331.